Using of Sentinel 2 Images for Tropical Economic Crops Growth Modeling

Totsanat Rattanakaew [1]

[1] Division of Policy and Land Use Planning, Land Development Department, Ministry of Agriculture and Cooperatives, Thailand - totsanat@yahoo.com

Keywords: Sentinel 2, Tropical Crops, Vegetation Index, Modeling, Crop Growth.

Abstract

Nowadays, a rapid advancement of remote sensing technology has led to widespread recognition of its potential to improve the efficiency and reliability of crops inspection and monitoring. The objectives of this project are 1. To create a database of annual remote sensing data of economic crops from satellite imagery, 2. To study the cultivation patterns of economic crops based on annual changes in reflectance values. 3. To study the relationship between spectral signatures and growth characteristics obtained from field surveys. The remote sensing data from Sentinel 2 were calculated vegetation indices such as Normalized Difference Vegetation Index (NDVI), Green Normalized Difference Vegetation Index (GNDVI) and Normalized Difference Infrared Index (NDII) to study the correlation with crops growth parameters of five economic crops of Thailand such as sugarcane, cassava, pineapple, oil palm, and para rubber. The results show that spectral reflectance of each crop change all year round and synchronized with growth data such as height, canopy width, stem size, and leaves chlorophyll content. Therefore, the remote sensing data has a potential for the 5 economic tropical crops growth and health monitoring. The satellite imagery from some month can be used to create crop growth assessment models including height, canopy width, and stem size and leaves chlorophylls content. In addition, the effectiveness of the model depends on the type of vegetation index used.

1. Introduction

The use of remote sensing technology, which acquires data through the collection of reflectance values from various objects on Earth, plays a critical role in managing and enhancing agricultural and agribusiness activities (Navalgund et al., 2007; Sowmya et al., 2017; Onojeghuo et al., 2018; Onojeghuo et al., 2021; GISGeography, 2022; Pakdel-Khasmakhi, 2022; Kyriakos and Vavalis, 2023). Currently, remote sensing technology has advanced significantly, particularly in satellite imagery and unmanned aerial vehicles (UAVs), offering higher spatial resolution and multi-spectral data acquisition capabilities (Liaghat and Balasundram, 2010; Kulo, 2018; Sishodia et al., 2020; Navalgund, 2001; Rattanakaew, 2018). This allows for the selection of appropriate spectral bands for various studies. Data from remote sensing serves as essential geospatial information in digital form, crucial for monitoring environmental and crop conditions due to its high quality, timebased analytical capability, and as a fundamental factor in creating and updating the national land use database. Thailand has an area of approximately 321 million rai (about 51.4 million hectares), with around 138 million rai (about 22.1 million hectares) dedicated to agriculture, constituting 43 percent of the national area. The agricultural sector plays a vital role in the economy, contributing to 6 percent of the national GDP and employing nearly a third of the workforce. Key export crops like sugarcane (Thailand being the world's second-largest sugar exporter), cassava (important in the animal feed and other industries), pineapple (significant in the food industry), rubber, and oil palm are crucial to both the economy and Thailand's global standing in these markets. Remote sensing technology is thus vital in supporting agriculture and agribusiness management, enabling stakeholders to monitor and manage production efficiently.

With remote sensing's capability for agricultural data analysis and monitoring, Thailand can enhance income security for farmers and the agribusiness sector. This benefits the management, study, and data preparation for remote sensing to support the analysis and monitoring of key crops in Thailand's economy, including sugarcane, cassava, pineapple, rubber, and oil palm. Effective remote sensing management of these crops directly benefits farmers by improving management strategies and increasing incomes. Both public and private sectors will be able to manage agricultural land more effectively, leading to enhanced productivity and economic growth.

2. Literature review

2.1 The Relevance of RS in Crop Growth Assessments

Crop growth can reflect to crop yield because it serves as an indicator of the plant's overall health and potential productivity. Healthy growth reflects adequate nutrient uptake, water availability, and favourable environmental conditions, all of which contribute to the development of more biomass, including the parts of the plant that are harvested. Crop growth study Traditionally, crop growth stages are observed from the ground, which is time-consuming and lacks spatial variability. Remote sensing Vegetation Index (VI) time series has been used to map land surface phenology (LSP) and relate to crop growth stages mostly after the growing season.

Currently, remote sensing technology is increasingly being applied to study plant growth. This approach utilizes the differences in reflection and absorption of energy by plants across various wavelengths to calculate the band ratio of electromagnetic energy, known as Vegetation Indices. Vegetation Indices refer to calculations derived from specific spectral bands related to vegetation, where proportions of these bands are analysed to understand the interaction between electromagnetic energy from the sun and vegetation. This interaction reflects light differently across various times and conditions in agricultural areas. Vegetation indices are designed to enhance the data for better usability or to improve the clarity of the information relevant to the study. They can indicate the proportion of vegetation cover, the condition of the plants, and reveal the health and any abnormalities of vegetation in crop fields. In general, vegetation index values can be adapted for diverse applications depending on the research objectives. Examples of commonly used indices include the Normalized Difference Vegetation Index

https://doi.org/10.5194/isprs-archives-XLVIII-M-6-2025-233-2025

(NDVI) (Rouse et al., 1974; Thompson et al., 2015), the Green Normalized Difference Vegetation Index (GNDVI) (Gitelson et al., 1996), and the Normalized Difference Infrared Index (NDII) (Hunt and Rock, 1989). These indices are valuable for real-time monitoring of crop growth, predicting or assessing characteristics such as leaf area, biomass, crop health, and vegetation density. These applications can be beneficial in various contexts, such as assessing seedling conditions (before and during planting stages), efficiently timing management techniques to ensure crop survival and yield, or promoting sustainable practices. Additionally, vegetation indices are useful in applications related to climate change impacts, especially regarding drought and extreme events like heat waves increasingly affecting drought-prone regions (Mongkonsawat, 1997).

(a) Normalized Difference Vegetation Index (NDVI) is a popular index for indicating vegetation greenness, density, and health on each pixel of a satellite image. NDVI has been widely used in remote sensing since its introduction in the 1970s, especially in digital agriculture. It uses the reflectance ratio between near-infrared (NIR) and red wavelengths, normalized to yield values between -1 and 1. Values close to 0 suggest a lack of green vegetation, while values around 0.8 or 0.9 indicate dense green vegetation. Areas covered with vegetation reflect more in the NIR than in the red spectrum, resulting in a positive NDVI, while bare soil shows similar reflectance in both bands, resulting in values near 0. Water surfaces, which reflect less in the NIR than in the red spectrum, result in negative values. Typically, NDVI values range from 0.1 to 0.7, making it effective for estimating plant vigour throughout the growing cycle by analysing the plant's spectral reflection. NDVI enables comparisons over time to track growth patterns. Understanding NDVI helps in evaluating plant health and differentiating between healthy and stressed plants based on chlorophyll and structural density. NDVI relies on energy and light reflection, with NIR and red bands providing a dimensionless indicator between -1 and 1. Plants appear green due to chlorophyll, which reflects green light while absorbing red, thus a healthy plant with ample chlorophyll and cell structure reflects NIR during photosynthesis. On our platform, the scale on the right side of the field references crop vigour. Satellite sensors in space capture light wavelengths absorbed and reflected by green plants, making NDVI ideal for analysing vegetation. NDVI values help detect and quantify live green vegetation by measuring reflectance in the visible and near-infrared bands, as defined by the standard NDVI formula (Gao, 1996).

(b) Green Normalized Difference Vegetation Index (GNDVI) is an index measuring vegetation greenness based on the difference between NIR and the green band in the electromagnetic spectrum, developed by Gitelson et al. (1996). GNDVI is more sensitive to chlorophyll variations in plants than NDVI and has a higher saturation point, making it suitable for dense vegetation or advanced growth stages. While NDVI is effective for early-stage vigour estimation, GNDVI serves as a photosynthesis activity indicator and a chlorophyll index, increasingly used to assess water and nitrogen levels in plant canopies due to its slower saturation compared to NDVI. As a widely used vegetation index, chlorophyll concentration serves as a key biomarker for various physiological processes linked to plant health, photosynthetic capacity, and stress detection, including drought stress. GNDVI values, ranging from -1 to 1, associate values between -1 and 0 with water presence or bare land. This index is primarily applied in the mid and late stages of the crop growth cycle.

(c) Normalized Difference Infrared Index (NDII) is an index that measures reflectance by calculating the difference between the near-infrared (NIR) and shortwave infrared (SWIR) wavelengths, developed by Hunt and Rock (1989). The NDII uses the same calculation formula as the Normalized Difference Water Index (NDWI) introduced by Gao (1996) or the Normalized Difference Moisture Index (NDMI) (Sentinel Hub, 2017). NDII is sensitive to changes in water content in plant canopies (Ji et al., 2011) and can effectively detect water stress in vegetation. This sensitivity is due to the properties of SWIR reflectance, which shows a negative relationship with leaf water content, as water is strongly absorbed by leaves. The index values increase with rising water content, making it applicable for agricultural crop management, forest canopy monitoring, and detecting plant stress (Hardisky et al., 1983; Sentinel Hub, 2017). NDII can also detect root-zone water stress due to its sensitivity to vegetation water status.

Because of this high sensitivity to plant water content, NDII provides more detailed information about vegetation conditions than NDVI. NDII shows a strong correlation with soil moisture in root zones at regional scales (Ochoa et al., 2022). The shortwave infrared wavelengths capture changes in both plant water content and the structure within the spongy mesophyll layer of plants, while NIR reflectance is influenced by internal leaf structure and leaf dry matter content, but not by water content. The combined analysis of NIR and SWIR wavelengths helps to remove variability caused by leaf structure and dry matter content, enhancing the accuracy of water content data extraction. The amount of water within the internal leaf structure largely governs electromagnetic reflectance in the SWIR range, meaning SWIR reflectance has a negative correlation with leaf water content. Thus, NDII can be used to track changes in leaf water content over time (Sentinel Hub, 2017). NDII values range from -1 to 1, with typical values for green vegetation lying between 0.02 and 0.6 (Hardisky et al., 1983; Sentinel Hub, 2017).

No.	VIs	Formula	References
a	NDVI	(NIR - red) / (NIR + red)	Rouse et al., 1974
b	GNDVI	(NIR - Green) / (NIR + Green)	Gitelson et al., 1996
c	NDII	(NIR - SWIR) / (NIR + SWIR)	Hunt and Rock, 1989

Table 1. Various Vegetation Indices.

This study hypothesizes that different plant species and growth stages exhibit variations in light absorption and reflection across both visible and non-visible wavelengths. Remote sensing data, which captures images across multiple wavelengths—including visible and non-visible spectra—are commonly used to calculate vegetation indices. These indices effectively analyze relationships with various growth parameters, enabling applications such as plant species classification, growth stage identification, and growth rate estimation.

Vegetation index values vary throughout the year, particularly for crops with planting-harvest-replant cycles. For instance, perennial crops tend to have higher vegetation indices like NDVI and GNDVI compared to seasonal crops. After harvesting, croplands exhibit low NDVI and GNDVI values, which gradually increase as new crops are planted and grow. However, remote sensing data collection for the growth stages of five key economic crops remains limited.

Studying monthly variations in vegetation indices not only reveals growth stages but also provides reference statistics for crop area classification using both visual and computer-based methods. This is particularly relevant in areas with small, mixed crop plots, such as cassava and sugarcane fields, where farmers often intersperse or rotate crops across plots. Satellite imagery classification in such cases can be challenging without experienced interpreters. These data can serve as a database for less experienced analysts and as thresholds for computer-based classification, especially in multi-temporal analysis using

https://doi.org/10.5194/isprs-archives-XLVIII-M-6-2025-233-2025

decision tree models. This approach enhances the accuracy of mapping five key economic crops.

Modeling relationships using regression equations is a popular method to correlate plant growth parameters—such as height and canopy width—with remote sensing data from reference plots. This method facilitates growth analysis and yield estimation. Growth parameters are treated as dependent variables, while remote sensing data serve as independent variables. The resulting models can predict growth parameters for adjacent plots by substituting vegetation index values into the equations, significantly reducing time and field data collection costs. Satellite imagery covers large areas and is easily analyzed with geospatial technology software, this approach is well-suited for studying plant abnormalities in extensive areas, forecasting growth, and estimating yields quickly. Such near real-time data allow relevant agencies to efficiently manage operations, such as plot management, input use, and production planning.

2.2 Sentinel 2

The Sentinel satellites are a series of natural resource monitoring satellites developed by the European Space Agency (ESA). This initiative was developed as part of the nextgeneration Earth observation missions under the Copernicus program, a collaborative effort between ESA and the European Commission. The aim of the Sentinel program is to replace older Earth observation missions, such as the ERS and Envisat missions, which have been decommissioned or are nearing the end of their operational lifespan. This ensures continuity of data without any gaps, supporting ongoing studies. Each mission focuses on various aspects of Earth observation, such as monitoring the atmosphere, oceans, and land. The data collected is applied in a wide range of applications (European Space Agency, 2022).

Sentinel-2 is part of the Copernicus program, the largest Earth observation program overseen by the European Commission in collaboration with ESA under the Global Monitoring for Environment and Security (GMES) program. Its objective is to enhance the EU's capacity to provide and utilize environmental and security-related information. Sentinel-2 is a wide-swath satellite designed to capture continuous imagery of the Earth's surface, building on data continuity from the Landsat and SPOT satellites. Launched into orbit in 2015, Sentinel-2 consists of two Earth observation satellites, Sentinel-2A and Sentinel-2B. These satellites capture solar reflectance data from the Earth's surface, operating in sun-synchronous orbits with a 180-degree phase difference, at an altitude of 786 kilometers. They monitor variations in land surface conditions with an image swath width of 290 kilometers and revisit the same area every 10 days at the equator with a single satellite, or every 5 days with two satellites under cloud-free conditions (2-3 days at midlatitudes). This enables tracking of surface changes on Earth (European Space Agency, 2022).

The mission of Sentinel-2 provides continuous imaging, transmitting data to ground stations every 5-7 days. It is valuable for terrestrial and marine monitoring, natural disaster mapping, and maritime vessel detection. The multispectral instrument (MSI) on board records reflectance data across 13 spectral bands, including visible light, near-infrared, and shortwave infrared bands, with spatial resolutions ranging from 10 to 60 meters. Sentinel-2 captures continuous imagery, transmitting data to ground stations every 5-7 days. Sentinel-2 is grouped by spatial resolution (Table 2): 10-meter resolution for four bands (bands 2, 3, 4, and 8); 20-meter resolution for six bands (bands 5, 6, 7, 8A, 11, and 12); and 60-meter resolution for three bands (bands 1, 9, and 10) (European Space Agency, 2022).

Band	Wavelength	Wavelength (αm)	Resolution (m)
1	Coastal aerosol	0.443	60
2	Blue	0.490	10
3	Green	0.560	10
4	Red	0.665	10
5	Vegetation Red Edge	0.708	20
6	Vegetation Red Edge	0.740	20
7	Vegetation Red Edge	0.783	20
8	Near Infrared	0.842	10
8A	Vegetation Red Edge	0.865	20
9	Water vapour	0.945	60
10	SWIR - Cirrus	1.375	60
11	SWIR	1.610	20
12	SWIR	2.190	2

Table 2. Sentinel 2 image. Source: European Space Agency (2022).

3. Methodology

1. Site selection: The selection of the operational area is based on choosing sub-watersheds that primarily have areas for growing five economic crops, namely sugarcane, cassava, pineapple, rubber, and oil palm.
2. Data Gathering: Collect a geospatial database and other relevant data related to the cultivation of the five major economic crops
3. Study Areas selection: Select study plots within the subwatershed under study to be used as reference plots for the study of wave signature values and the collection of data on plant growth changes throughout the year. The steps are as follows:

3.1 Selection of Reference Plots: Reference plots are selected using systematic sampling, with the plots chosen based on the type of crop to ensure distribution across the subwatershed being studied.

3.2 Selection of Reference Plots for Each Crop Using Purposive Sampling, Considering Plots with Sizes Ranging from 10 to 50 Rai.

https://doi.org/10.5194/isprs-archives-XLVIII-M-6-2025-233-2025

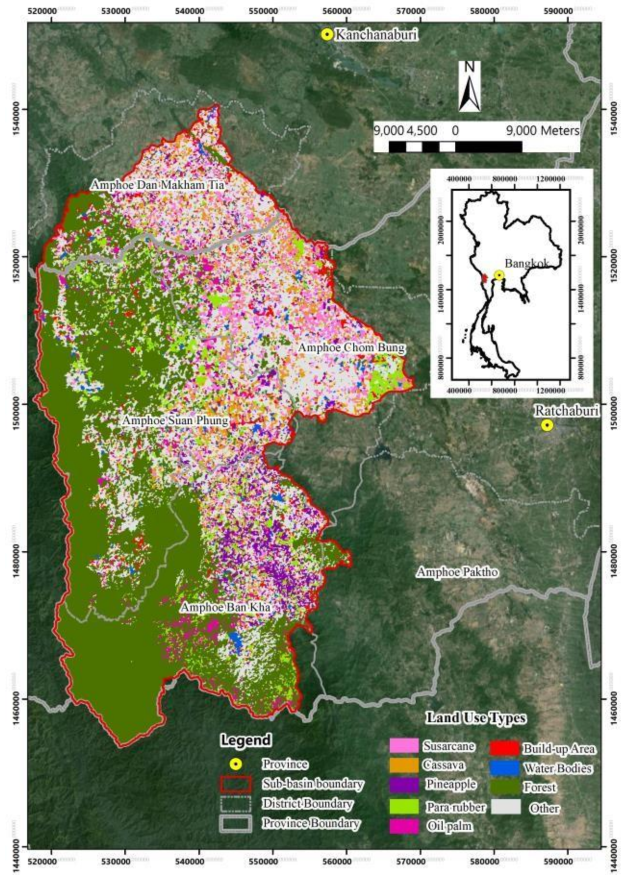

Figure 1. Distribution areas of five economic crops in Lam Phachi Sub-Basin.

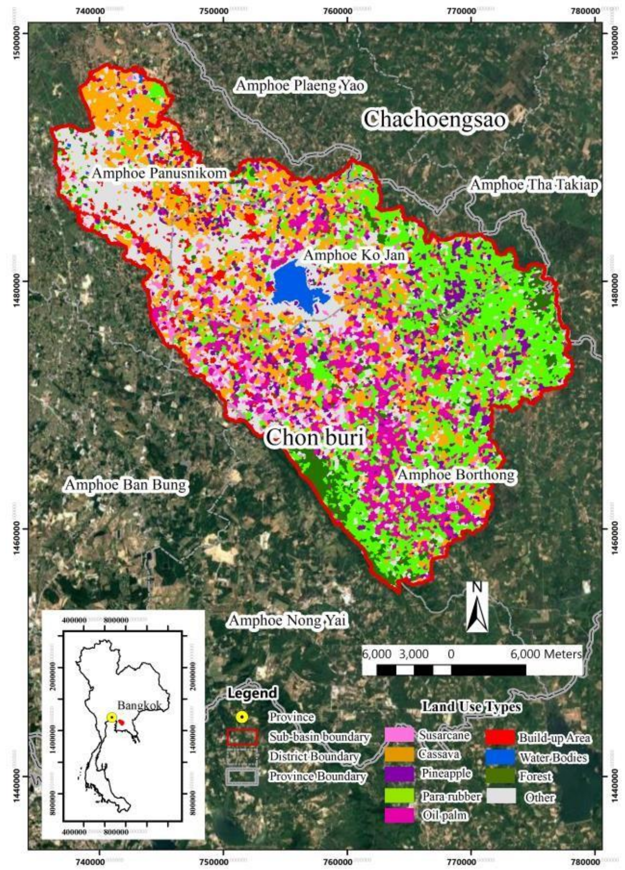

Figure 2. Distribution areas of five economic crops in Khlong Luang Sub-Basin.

4. Collect data and prepare Sentinel 2 satellite imagery of the COPERNICUS/S2 type for the Lam Phachi Sub-Basin and Khlong Luang Sub-Basin by calculating three vegetation indices: NDVI, GNDVI, and NDII through https://code.earthengine.google.com/. The resulting values will be the monthly median value for each month of the study year.
5. Field Data Collection: Conduct surveys and collect plant data in reference plots, including height, canopy width, stem diameter, and chlorophyll content using the SPAD-502 chlorophyll meter by Konica Minolta. The plant data will be randomly sampled from five plants per plot to calculate the average. The plants selected for sampling will be those that exhibit similar growth patterns across the entire plot, with sampling points spread evenly throughout the plot.
6. Analyze the relationship between reflectance data and field data using a regression model, considering the correlation values from the p-value and r-square.

4. Results

The creation of a database to study the cropping patterns of economically significant plants through annual spectral reflectance changes revealed that the reflectance values of five plant species varied distinctly throughout the year. By applying regression analysis to investigate the relationship between spectral signatures and morphological characteristics of these five economic plants, it was found that three vegetation indices were correlated with morphological attributes, including plant height, canopy width, stem size, and chlorophyll content in leaves. The type of equation used and the data periods analyzed affected the resulting r2 and p-values of the model. Generally, incorporating multiple vegetation indices in a multiple linear regression equation enhanced the correlation between spectral signatures and morphological attributes, with the highest correlations observed in each model. These models can be further used to estimate the growth and health status of the five plant species. The detailed study results are as follows:

4.1 Sugarcane

The reflectance values exhibit clear changes throughout the year. During the period after harvest when the crop is either waiting to sprout again or being replanted (February-March), the vegetation index is at its lowest. It then steadily increases as the sugarcane starts to sprout (April-May) and continues through the growth stage (June-September). The vegetation index peaks near harvest time (October-November) and decreases during the harvesting period (December-January), reaching its lowest again after harvest, completing the annual cycle. However, the physiological characteristics and reflectance values of sugarcane exhibit considerable variability between January and March, due to some fields having already been harvested while others have not. The changes in the physiological characteristics and reflectance values follow a clear pattern, which can be attributed to the defined planting period for sugarcane, as planting must align with the factory's designated purchasing periods. Therefore, reflectance values can be used to study the sugarcane planting cycle and to classify areas where sugarcane is sprouting, standing, harvested, or awaiting new growth. The highest correlation between spectral signatures and the physiological characteristics of sugarcane each year is shown in Table 3 and 4.

Year	Month	Equation	r^2
Height			
2021	Apr	H = -223.418 + 910.22b - 29.836c	0.61**
2022	Feb	H = 270.387 + 49.330a+ 1224.933c	0.47**
2023	Mar	H = 19.507 + 930.483a+ 800.599c	0.65**
Canopy Width			
2021	-	-	-
2022	Feb	W = 64.923 + 343.714a + 301.348c	0.60**
2023	Sep	W =194.598 -131.087a	0.44**
Stem Size			
2021	-	-	-
2022	-	-	-
2023	-	-	-
Leaf chlorophylls Content			
2021	Apr	CHLO = 56.871 + 131.087a - 209.544b -35.863c	0.75**
2022	-	-	-
2023	-	-	-

Table 3. The highest correlation between spectral signatures and biometric parameters of sugarcane in Lam Phachi Sub-Basin.
Remarks: a = NDVI, b = GNDVI, c = NDII
* = $p < 0.05$, model inefficint less than 5%
** = $p < 0.01$, model inefficint less than 1%

Year	Month	Equation	r^2
Height			
2021	Sep	H = 192.649 + 290.256c	0.43*
2022	Mar	H = -9.455 + 358.269a - 41.646c	0.56**
2023	Jun	H = 124.581 -506.648a +548.658b + 227.280c	0.75**
Canopy Width			
2021	May	W = 82.432 + 53.421a + 136.621c	0.49**
2022	Apr	W = 7.773 -48.975a + 40.975b + 453.045c	0.56**
2023	Jun	W = 133.899 -277.437a + 312.377b + 141.206c	0.73**
Stem Size			
2021	May	SZ = 3.203 + 2.967a + 6.170c	0.52**
2022	Oct	SZ = 1.253 + 0.622a + 4.855b	0.33**
2023	-	-	-
Leaf chlorophylls Content			
2021	Aug	CHLO = 38.792 + 31.250c	0.47**
2022	Mar	CHLO = 27.664 + 50.645b	0.34**
2023	Jun	CHLO = 32.325 -19.958a + 42.991b + 5.648c	0.62*

Table 4. The highest correlation between spectral signatures and biometric parameters of sugarcane in Khlong Luang Sub-Basin.
Remarks: a = NDVI, b = GNDVI, c = NDII
* = $p < 0.05$, model inefficint less than 5%
** = $p < 0.01$, model inefficint less than 1%

4.2 Cassava

It was found that the period from February to April is when the vegetation index of the cassava planting fields is at its lowest. This is due to the fact that during this period, most farmers have not yet planted cassava cuttings, or if they have, the cassava has not yet sprouted. As a result, the vegetation index during this time behaves similarly to the reflectance values or soil vegetation index. The vegetation index begins to increase from May to November because there are cassava plants that are actively growing in the fields during this time. The vegetation index starts to decline from December to January as farmers begin harvesting, and it reaches its lowest point in February when the cassava has been fully harvested. The highest correlation between the spectral signature and the phenological values of cassava each year is shown in Table 5 and 6.

Year	Month	Equation	r^2
Height			
2021	-	-	-
2022	-	-	-
2023	Jun	H = -10.886 + 61.360a + 248.342b + 161.524c	0.46**
Canopy Width			
2021	Dec	W = -58.607 + 344.490b - 115.757c	0.46**
2022	Jan	W = -65.159 + 216.072a + 439.681b	0.47**
2023	Jun	W = 34.796 + 603.498a - 491.880b -148.22c	0.57**
Stem Size			
2021	Apr	SZ = -0.267 + 5.250a	0.44**
2022	-	-	-
2023	Jul	SZ = -0.076 + 3.825a	0.48**
Leaf chlorophylls Content			
2021	-	-	-
2022	-	-	-
2023	Sep	CHLO = 27.409 + 62.755b	0.70**

Table 5. The highest correlation between spectral signatures and biometric parameters of Cassava in Lam Phachi Sub-Basin.
Remarks: a = NDVI, b = GNDVI, c = NDII
* = $p < 0.05$, model inefficint less than 5%
** = $p < 0.01$, model inefficint less than 1%

Year	Month	Equation	r^2
Height			
2021	Sep	H = -402.443 + 768.175a + 101.832b	0.54**
2022	Mar	H = 156.137 -336.411c	0.28**
2023	Mar	H = -55.573 + 445.814a + 172.247b + 134.866c	0.79**
Canopy Width			
2021	Sep	W = 14.860 +96.559a + 123.781c	0.74**
2022	Mar	W = -7.255 + 152.079a + 88.336b	0.76**
2023	Mar	W = 25.707 + 83.987a + 66.456b + 46.871c	0.54**
Stem Size			
2021	Dec	SZ = 0.983 -3.084a + 3.659b + 4.842c	0.40**
2022	Jul	SZ = -0.387 + 3.811a + 1.845b	0.72**
2023	Mar	SZ = -0.044 + 3.603a + 1.544b + 0.987c	0.50**
Leaf chlorophylls Content			
2021	-	-	-
2022	Jun	CHLO = 58.364 -32.586a	0.31**
2023	Mar	CHLO = 37.153 + 27.288a + 4.258b + 8.477c	0.65**

Table 6. The highest correlation between spectral signatures and biometric parameters of Cassava in Khlong Luang Sub-Basin.
Remarks: a = NDVI, b = GNDVI, c = NDII
* = $p < 0.05$, model inefficint less than 5%
** = $p < 0.01$, model inefficint less than 1%

4.3 Pineapple

The comparison of the average 5-year reflectance values or vegetation index (VI) in each month for pineapple with the 5-year average vegetation index in each month for sugarcane and cassava shows that the vegetation index values for pineapple tend to be higher. The NDVI values ranged from 0.365 to 0.560, the GNDVI values ranged from 0.350 to 0.471, and the NDII values ranged from 0.063 to 0.197. It was found that the vegetation index values for pineapple tend to be higher in months with more rainfall and lower in months with less rainfall, similar to the variation in chlorophyll levels. Therefore, it may be possible that the three vegetation indices have the potential to estimate the chlorophyll content in pineapple leaves and can be used to predict water stress and water requirements for pineapples. The use of satellite imagery, particularly from Sentinel 2, which provides data every 10 days, allows for the calculation of the average monthly vegetation index over 5 years for reference plots, which can also be used to study the growth cycle of pineapple, just as it has been done for sugarcane and cassava.

The average 5-year monthly vegetation index values can be divided into two periods. The first period, from February to April, is when the vegetation index values in the pineapple fields are lower. The average NDVI values range from 0.365 to 0.374, the average GNDVI values range from 0.350 to 0.364, and the average NDII values range from 0.063 to 0.071. This period corresponds to the dry season, when farmers harvest and wait for rainfall to enable further growth of the pineapple or prepare the fields for replanting. The second period, from May to January, is when the vegetation index values in the pineapple fields are higher. The average NDVI values range from 0.417 to 0.560, the average GNDVI values range from 0.376 to 0.471, and the average NDII values range from 0.105 to 0.197. This period aligns with the changes in chlorophyll levels in the leaves each month. The highest correlation between the spectral signature and the physiological characteristics of pineapple in each year is shown in Table 7 and 8.

Year	Month	Equation	r^2
Height			
2021	Dec	H = -6.231 + 103.587a + 22.435b	0.49**
2022	Feb	H = 46.733 + 104.034c	0.57**
2023	Jul	H = 73.381 -53.024a -29.606b -22.734c	0.56*
Canopy Width			
2021	May	W = 43.302 + 14.822b +93.349c	0.43**

2022	Apr	W = -8.439 + 140.712a + 118.825b -41.792c	0.48*
2023	-	-	-
Leaf chlorophylls Content			
2021	Jul	CHLO = 109.338 -97.203a	0.38**
2022	Feb	CHLO = 56.850 -124.543a + 102.652b + 90.633c	0.43*
2023	Dec	CHLO = 30.850 + 72.856b	0.41**

Table 7. The highest correlation between spectral signatures and biometric parameters of Pineapple in Lam Phachi Sub-Basin.

Remarks: a = NDVI, b = GNDVI, c = NDII
* = $p < 0.05$, model inefficint less than 5%
** = $p < 0.01$, model inefficint less than 1%

Year	Month	Equation	r^2
Height			
2021	Aug	H = -14.381 + 107.865a + 84.108Gb	0.68*
2022	Jan	H = 47.634 + 349.591a 328.243b + 17.488c	0.58**
2023	Aug	H = -30.795 -172.743a+ 425.012b + 14.915c	0.67**
Canopy Width			
2021	May	W = 127.770 -61.712a 109.046b	0.60*
2022	Jan	W = 19.144 + 390.892a268.330b -46.522c	0.81**
2023	Aug	W = -57.923 -258.945a+ 658.340b	0.74**
Leaf chlorophylls Content			
2021	-	-	-
2022	-	-	-
2023	Aug	CHLO = 32.486 + 44.735a + 13.769b + 47.611c	0.55*

Table 8. The highest correlation between spectral signatures and biometric parameters of Pineapple in Khlong Luang Sub-Basin.

Remarks: a = NDVI, b = GNDVI, c = NDII
* = $p < 0.05$, model inefficint less than 5%
** = $p < 0.01$, model inefficint less than 1%

4.4 Para Rubber

The rubber tree's Vegetation Index (NDVI) from January to April typically has a lower average value, ranging from 0.436 to 0.540. This is consistent with the lower chlorophyll content in the leaves during this period, as it coincides with the dry season. During this time, the rubber tree leaves change color and shed. The Vegetation Index of rubber gradually increases from May to November, which is the rainy season, allowing the rubber tree to sprout new leaves. The leaves and trees grow well due to adequate water availability, and the leaves accumulate higher levels of chlorophyll. The NDVI ranges from 0.536 to 0.678 during this period. However, in August, the 5-year average NDVI decreases slightly, which may be due to reduced rainfall from June to August, affecting the water supply to the rubber trees and potentially impacting their growth. Rubber trees are perennial plants, but their growth cycle is closely linked to the seasons and the amount of water they receive, similar to pineapples. The study's results suggest the potential to estimate chlorophyll content and predict water stress and water requirements for rubber trees. Additionally, it was found that the Vegetation Index of rubber is higher than that of sugarcane, cassava, and pineapple. The highest correlation between the spectral signatures and the physiological values of rubber trees in each year is shown in Table 6.

Year	Month	Equation	r^2
Height			
2021	Apr	$H = 932.41e^{2.797C}$	0.64**
2022	Mar	$H = 9695.4b^{1.7486}$	0.43**
2023	Apr	H = 1914.179 + 3478.520a - 6061.918b + 5096.662c	0.40**
Canopy Width			
2021	Apr	$W = 456.97e^{2.1234c}$	0.58**
2022	Mar	$W = 463.89e^{2.4051c}$	0.34**
2023	Apr	$W = 1309.2a^{0.6185}$	0.36**
Stem Size			
2021	Apr	SZ = 56.824 - 258.560a + 246.777b + 132.052c	0.48**
2022	Mar	SZ = 112.61b + 17.316	0.27**
2023	Apr	SZ = 36.239 - 14.868a + 81.316b + 31.636c	0.49**
Leaf chlorophylls Content			
2021	Nov	CHLO = 34.424 - 12.529a + 56.203b + 36.385c	0.81**
2022	Jan	CHLO = 104.43c + 40.424	0.52**
2023	Apr	CHLO = 32.700 + 75.819a - 23.270b - 17.091c	0.39**

Table 9. The highest correlation between spectral signatures and biometric parameters of Para rubber in Lam Phachi Sub-Basin.

Remarks: a = NDVI, b = GNDVI, c = NDII
* = $p < 0.05$, model inefficint less than 5%
** = $p < 0.01$, model inefficint less than 1%

Year	Month	Equation	r^2
Height			
2021	Apr	H = 382.595 + 1035.323a + 70.241b + 1933.167c	0.28**
2022	Mar	H = -17.878 + 1271.153a + 1968.876b + 3716.948c	0.34**
2023	Apr	H = 584.046 + 1625.316a + 2368.925b + 2992.900c	0.79**
Canopy Width			
2021	Apr	W = 144.093 + 559.844a + 405.947b + 160.288c	0.34**
2022	Mar	W = 161.532 + 732.263a + 432.353b + 1117.480c	0.43**
2023	Apr	W = 411.806 + 598.446a + 749.956b + 1023.525c	0.59**
Stem Size			
2021	Apr	SZ = 13.930 + 38.923a + 14.214b + 38.079c	0.33**
2022	Mar	SZ = 1.069 + 55.326a + 63.460b + 55.384c	0.38**
2023	Apr	SZ = 25.458 + 44.23a + 66.522b + 72.683c	0.63**
Leaf chlorophylls Content			
2021	Nov	CHLO = 55.476 -28.143a+ 45.837b -37.117c	0.61**
2022	Jan	CHLO = 33.940 + 8.640a + 1.250b + 72.015c	0.48*
2023	Apr	CHLO = 43.730 + 12.274a + 13.934b + 11.368c	0.58**

Table 10. The highest correlation between spectral signatures and biometric parameters of Para rubber in Khlong Luang Sub-Basin.

Remarks: a = NDVI, b = GNDVI, c = NDII
* = $p < 0.05$, model inefficint less than 5%
** = $p < 0.01$, model inefficint less than 1%

4.5 Oil Palm

The vegetation index of oil palm during the period from February to April has an average NDVI value that is low, ranging from 0.476 to 0.488, which corresponds to lower chlorophyll content in the leaves compared to other periods. This is due to the dry season, where water may be insufficient for the growth of oil palm. The vegetation index of oil palm gradually increases from May to November, which is the rainy season, allowing the leaves and trees to grow well due to sufficient water, and chlorophyll content in the leaves increases. Since oil palm is a perennial plant, its growth cycle is aligned with the seasons and the amount of water it receives, similar to pineapple and rubber trees. The findings of this study may have potential for estimating chlorophyll content and predicting water stress and water requirements of oil palm. Additionally, it was found that the vegetation index of oil palm is higher than that of sugarcane, cassava, and pineapple, which are crops grown in smaller fields. However, when compared with the vegetation index of rubber, which is also a perennial plant, the vegetation index of oil palm tends to be higher during the season. Moreover, the five-year average NDII index of oil palm is significantly higher than other crops, as oil palm has a large canopy, is evergreen, and continuously covers the field, resulting in a higher NDII value. The highest correlation between spectral signatures and physiological characteristics of oil palm each year is shown in Table 7.

Year	Month	Equation	r^2
Height			
2021	-	-	-
2022	Mar	H = -15.562 + 967.428a +789.795b + 1781.790c	0.55**
2023	Apr	H = 1342.830 -5288.715a + 3128.109b + 4846.635c	0.44**
Canopy Width			
2021	-	-	-
2022	Mar	W = 1272.893 + 625.177a - 1443.405b+ 443.083c	0.54**
2023	Apr	W = 491.227 + 196.636a + 692.451b + 866.515c	0.40**
Stem size			
2021	-	-	-
2022	Mar	SZ = 194.176 -465.993a + 265.040b + 423.888c	0.56**
2023	Apr	SZ = 150.612 + 177.864a + 84.278b + 49.913c	0.42**
Leaf chlorophylls Content			
2021	Dec	CHLO = 43.201 + 3.824a + 29.457b + 21.444c	0.53**
2022	Feb	CHLO = 64.424 -78.008a + 116.943b + 17.131c	0.59**
2023	May	CHLO = 35.718 -140.649a + 247.959b + 37.816c	0.85**

Table 11. The highest correlation between spectral signatures and biometric parameters of Oil Palm in Lam Phachi Sub-Basin.

Remarks: a = NDVI, b = GNDVI, c = NDII
* = $p < 0.05$, model inefficint less than 5%
** = $p < 0.01$, model inefficint less than 1%

Year	Month	Equation	r^2
Height			
2021	Apr	H = 421.316 + 326.211a+ 394.315b + 1059.954c	0.39**
2022	Mar	H = -816.622 + 3195.892a+ 2466.027b + 2285.257c	0.47**
2023	Apr	H = 309.621 + 1144.942a + 2431.173b + 2763.557c	0.60**
Canopy Width			
2021	Apr	W = 590.044 + 181.329a + 323.117b + 317.041c	0.47**
2022	Mar	W = 496.838 + 345.181a + 761.124b + 651.668c	0.43**
2023	Apr	W = 885.148 + 118.064a + 477.726b + 420.063c	0.51**
Stem size			
2021	Apr	SZ = 176.603 + 65.584a + 46.989b + 23.746c	0.39**
2022	Mar	SZ =199.853 -9.476a + 84.390b + 166.812c	0.42**
2023	Apr	SZ = 206.797 + 146.412a - 21.797b + 71.173c	0.54**
Leaf chlorophylls Content			
2021	Dec	CHLO = 85.579 -11.070a - 8.920b -10.220c	0.53**
2022	Apr	CHLO = 57.078 + 9.144a + 22.731b + 25.886c	0.55**
2023	Apr	CHLO = 61.466 + 13.966a + 12.831b + 22.031c	0.68**

Table 12. The highest correlation between spectral signatures and biometric parameters of Oil Palm in Lam Phachi Sub-Basin.
Remarks: a = NDVI, b = GNDVI, c = NDII
* = $p < 0.05$, model inefficint less than 5%
** = $p < 0.01$, model inefficint less than 1%

5. Summary

5.1 Developing an Annual Remote Sensing Database for Key Crops Using Satellite Imagery with Google Earth Engine: Satellite imagery is collected and mosaicked using Google Earth Engine to generate monthly images, enabling annual phenological monitoring of five crop types. This database can serve as a foundation for creating localized crop calendars, providing insights into planting and harvest timings. It also aids in estimating cultivated areas and forecasting harvestable land for these economic crops.
5.2 Vegetation Index Variability as an Indicator of Phenological Changes: The vegetation index varies over time, corresponding to phenological changes, such as plant height and canopy width. These characteristics, consistent year by year, enable assessment of crop health annually. For example, in years with adverse weather, like low rainfall, poor crop growth is observed, reflected in lower vegetation indices such as NDVI and GNDVI compared to years with favourable weather conditions. 5.3 Potential of Vegetation Indices in Modeling Crop Growth: Vegetation indices have the potential to create models assessing different growth parameters and can use satellite imagery from selected months for modeling. The three vegetation indices exhibit potential for modeling crop height, canopy width, stem size, and chlorophyll content, aiding in crop health assessment and growth prediction.

Acknowledgements

I would like to thank the Thailand Research Fund (TRF) and the Land Development Department of Thailand for their support in funding this project.

References

Azizan, F.A., Astuti, I.S., Aditya, M.I., Febbiyanti, T.R., Williams, A., Young, A., Abdul Aziz, A., 2021. Using multi-temporal satellite data to analyse phenological responses of rubber (Hevea brasiliensis) to climatic variations in South Sumatra, Indonesia. *Remote Sensing*, 13(15), 2932. https://www.mdpi.com/2072-4292/13/15/2932.

Chen, Y., Feng, L., Mo, J., Mo, W., Ding, M., Liu, Z., 2020. Identification of sugarcane with NDVI time series based on HJ-1 CCD and MODIS fusion. *Journal of the Indian Society of Remote Sensing*, 48(2), 249-262.

European Space Agency, 2022. SENTINEL 2 MISSION GUIDE. https://sentinel.esa.int/web/sentinel/missions/Sentinel 2, (10 April 2022)

Gao, B., 1996. NDWI -A Normalized Difference Water Index for Remote Sensing of Vegetation Liquid Water from Space. *Remote Sensing of Environment*, 58(3), 257-266.

Gao, F., Zhang, X., 2021. Mapping crop phenology in near real-time using satellite remote sensing: Challenges and opportunities. *Journal of Remote Sensing*.

GISGeography, 2022. 100 Earth Shattering Remote Sensing Applications & Uses. https://gisgeography.com/ remote-sensing-applications/ (23 December 2022).

Gitelson, A.A., Kaufman, Y.J., Merzlyak, M.N., 1996. Use of a green channel in remote sensing of global vegetation from EOS-MODIS. *Remote Sensing of Environment*, 58(3), 289-298.

Hardisky, M., Klemas, V., Smart, R., 1983. The influence of soil salinity, growth form, and leaf moisture on-the spectral radiance of Spartina Alterniflora Canopies. *Photogrammetric Engineering and Remote Sensing*, 49, 77-83.

Horticulture Research Institute, 2017. Quality Pineapple Production Management. Horticulture Research Institute, Department of Agriculture, Ministry of Agriculture and Cooperatives, Thailand. 184. [In Thai]

Hunt, E.R.Jr., Rock, B.N., 1989. Detection of changes in leaf water content using near- and middle-infrared reflectances. *Remote Sens. Environ.*, 30, 43–54. doi.org/10.1016/0034-4257(89)90046-1.

Ji, L., Zhang, L., Wylie, B.K., Rover, J., 2011. On the terminology of the spectral vegetation index (NIR−SWIR)/(NIR+ SWIR). *International Journal of Remote Sensing*, 32(21), 6901-6909.

Kulo, N., 2018. Benefits of the Remote Sensing Data Integration. Department of Geodesy and Geoinformatics, Faculty of Civil Engineering University of Sarajevo, Sarajevo, Bosnia and Herzegovina. https://www.researchgate.net/publication/329443299.

Kyriakos, C., Vavalis, M., 2023. Business Intelligence through Machine Learning from Satellite Remote Sensing Data. *Future Internet*, 15(11). doi.org/10.3390/fi15110355.

Liaghat, S., Balasundram, S.K., 2010. A review: The role of remote sensing in precision agriculture. *American Journal of Agricultural and Biological Sciences*, 5(1), 50-55.

Mishra, S., Jabin, S., 2020. Land Use Land Cover Change Detection using LANDSAT images: A Case Study. 2020 *IEEE 5th International Conference on Computing Communication and Automation (ICCCA)*, Galgotias University, Greater Noida, UP, India. Oct 30-31, 730-735.

Mongkonsawat, C., 1997. *Remote Sensing Survey*. Khon Kaen Printing Ltd. [in Thai]

Navalgund, R.R., 2001. Sensors and Platforms. Remote Sensing. Part 1. Basics and Applications, Resonance, 6(12), 51-60.

Navalgund, R.R., Jayaraman, V., Roy, P.S., 2007. Remote sensing applications: An overview. *Current Science*, 93(12), 1747-1766.

Ochoa, C.G., Villarreal-Guerrero, F., Prieto-Amparán, J.A., Garduño, H.R., Huang, F., Ortega-Ochoa, C., 2023. Precipitation, Vegetation, and Groundwater Relationships in a Rangeland Ecosystem in the Chihuahuan Desert, Northern Mexico. *Hydrology*, 10(2), 41. doi.org/10.3390/hydrolog y10020041.

Onojeghuo, A.O., Onojeghuo, A.R., Cotton, M., Potter, J., Jones, B., 2021. Wetland mapping with multi-temporal sentinel-1 &-2 imagery (2017–2020) and LiDAR data in the grassland natural region of alberta. *GIScience & Remote Sensing*, 58(7). doi.org/10.1080/15481603.2021.1952541.

Onojeghuo, A.O., Blackburn, G.A., Wang, Q., Atkinson, P.M., Kindred, D., Miao, Y., 2018. Mapping paddy rice fields by applying machine learning algorithms to multi-temporal Sentinel-1A and Landsat data. *International Journal of Remote Sensing*, 39(4), 1042-1067.

Pakdel-Khasmakhi, H., Vazifedoust, M., Paudyal, D.R., Chadalavada, S., Alam, M.J., 2022. Google Earth Engine as multi-sensor open-source tool for monitoring stream flow in the transboundary river basin: Doosti River Dam. *ISPRS International Journal of Geo-Information*, 11, 535. doi.org/10.3390/ijgi11110535.

Rahman, M.L., Rahman, S.H., 2021. Detection of land use land cover changes using remote sensing and GIS techniques in a secondary city in Bangladesh. *Grassroots Journal of Natural Resources*, 4(3), 132-146.

Rattanakaew, T., 2015. Application of Remote Sensing Technology for Nitrogen Fertilizer Management. *The Journal of the Thai Government Scholarship Students Association*, 138-145. [In Thai]

Remote Sensing: Challenges and Opportunities. *Journal of Remote Sensing*.

Rouse, J.W., Haas R.H., Schell, J.A., Deering, D.W., 1974. Monitoring vegetation systems in the Great Plains with ERTS. In: S.C. Freden, E.P. Mercanti, and M. Becker (eds) Third Earth Resources Technology Satellite–1 Syposium. Volume I: Technical Presentations, NASA SP-351, NASA, Washington, D.C., 309-317.

Scarpare, F.V.n.d. Sugarcane Phenology Phases. https://www.researchgate.net/figure/Sugarcanephenological-phases-relative-to-cropdevelopment_fig4_304315524.

Sentinel Hub, 2017. NDII (Normalized difference 819/1600). https://custom-scripts.sentinel-hub.com/customscripts/sentinel-2/ndii/#.

Simms, É.L. and Ward, H., 2013. Multisensor NDVI-based monitoring of the tundra-taiga interface (Mealy Mountains, Labrador, Canada). *Remote Sensing*, 5(3), 1066-1090. www.mdpi.com/journal/remotesensing.

Sishodia, R.P., Ray, R.L., Singh, S.K., 2020. Applications of remote sensing in precision agriculture: A review. *Remote Sensing*, 12(19), 3136. https://www.mdpi.com/2072-4292/12/19/3136.

Sowmya, D., Deepa, P., Venugopal, K., 2017. Remote Sensing Satellite Image Processing Techniques for Image Classification: A Comprehensive Survey. *International Journal of Computer Applications*, 161(11), 24-37.

Thompson, C.N., Guo, W., Sharma, B., Ritchie, G.L., 2019. Using normalized difference red edge index to assess maturity in cotton. *Crop Science*, 59(5), 2167-2177.